This is a repository copy of *Nighttime chemical transformation in biomass burning plumes : A box model analysis initialized with aircraft observations*.

White Rose Research Online URL for this paper:
https://eprints.whiterose.ac.uk/142616/

Version: Accepted Version

Article:

Supporting Information for Nighttime chemical transformation in biomass burning plumes: a box model analysis initialized with aircraft observations

Zachary C. J. Decker[1,2,3], Kyle J. Zarzana[1,2,3], Matthew Coggon[1,3], Kyung-Eun Min[1,3,†], Ilana Pollack[1,††], Thomas B. Ryerson[3], Jeff Peischl[1,3], Pete Edwards[4], William P. Dubé[1,3], Milos Z. Markovic[1,†††], James M. Roberts[1,3], Patrick R. Veres[3], Martin Graus[1,††††], Carsten Warneke[1,3], Joost de Gouw[1,2], Lindsay E. Hatch[5], Kelley C. Barsanti[5], Steven S. Brown[2,3,]*

[1]Cooperative Institute for Research in Environmental Sciences, University of Colorado, Boulder, Colorado, 80309, United States. [2]Department of Chemistry, University of Colorado, Boulder, Colorado 80309-0215, United States. [3]NOAA Earth System Research Laboratory (ESRL), Chemical Sciences Division, Boulder, Colorado 80305, United States. [4]Wolfson Atmospheric Chemistry Laboratories, Department of Chemistry, University of York, York YO10 5DD, United Kingdom. [5]Department of Chemical and Environmental Engineering and College of Engineering – Center for Environmental Research and Technology (CE-CERT), University of California, Riverside, California 92507, United States. [†]Now at Gwangju Institute of Science and Technology, School of Earth Sciences and Environmental Engineering, Gwangju, South Korea 61005. [††]Now at Colorado State University, Atmospheric Science Department, Ft. Collins, CO, USA 80523-1371. [†††]Now at Picarro inc, Santa Clara, CA, 95054. [††††]Now at the Department of Atmospheric and Cryospheric Sciences, University of Innsbruck, Austria 6020.
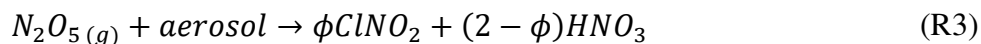
20   * steven.s.brown@noaa.gov

21   Abstract: Biomass burning (BB) is a large source of reactive compounds to the atmosphere. While

22   the daytime photochemistry of BB emissions has been studied in some detail, there has been little

23   focus on nighttime reactions despite the potential for substantial oxidative and heterogeneous

24   chemistry. Here we present the first analysis of nighttime aircraft intercepts of agricultural BB

25   plumes using observations from the NOAA WP-3D aircraft during the 2013 Southeast Nexus

26   (SENEX) campaign. We use these observations in conjunction with detailed chemical box

27   modeling to investigate the formation and fate of oxidants (NO_3, N_2O_5, O_3, and OH) and BB

28   volatile organic compounds (BBVOCs), using emissions representative of agricultural burns (rice

29   straw) and western wildfires (ponderosa pine). Field observations suggest NO_3 production was

30   approximately 1 ppbv hr^{-1}, while NO_3 and N_2O_5 were at or below 3 pptv, indicating rapid

31   NO_3/N_2O_5 reactivity. Model analysis shows that >99% of NO_3/N_2O_5 loss is due to BBVOC + NO_3

32   reactions rather than aerosol uptake of N_2O_5. Nighttime BBVOC oxidation for rice straw and

33   ponderosa pine fires is dominated by NO_3 (72, 53%, respectively) but O_3 oxidation is significant

34   (25, 43%) leading to roughly 55% overnight depletion of the most reactive BBVOCs and NO_2.

35   **Introduction**

36   Wildfire size and frequency in the Western U.S. has increased over the last 20 years, and these

37   trends are projected to continue due to factors such as forest management practices, elevated

38   summer temperatures, earlier snowmelt, and drought.[1,2] Biomass burning (BB), including

39   wildfires, prescribed burning, and agricultural burning, represents a large, imperfectly

40   characterized and chemically complex source of reactive material to the troposphere. BB releases

41   reactive species and particulate matter that impact the radiative balance of the atmosphere, air

42 quality, and human health on local to global scales.[3–7] The gas-phase components of BB plumes

43 include volatile organic compounds (BBVOCs) as well as nitrogen oxides (NO_x=NO+NO_2 and

44 higher oxides such as peroxyacyl and alkyl nitrates), oxidants, and oxidant precursors. The air

45 quality and climate effects of BB emissions are defined in part by the oxidative processes and

46 atmospheric chemical cycles that occur as the smoke is transported, diluted, and exposed to

47 oxidants over the hours and weeks following emission.

48   The photochemistry of BB plumes has been studied previously in a number of field and

49 laboratory studies. Daytime BB plumes can have OH concentrations 5-10 times higher than

50 background air[8] and daytime reactions of NO_x, BBVOCs, and OH involve complex pathways

51 that generally lead to O_3 formation, but in some cases to near-field O_3 titration.[9–14] Much less is

52 known about nighttime BB plume oxidative processes, which are expected to be dominated by

53 nitrate radicals (NO_3) and O_3.[15] NO_3 is formed by O_3 oxidation of NO_x (R1 & Figure 1) but is

54 rapidly (τ < 10 s) destroyed in the daytime by NO and photolysis.[15,16] NO_3 is a precursor for

55 N_2O_5 (R2), a NO_x reservoir. N_2O_5 may undergo heterogeneous uptake to form $ClNO_2$ and HNO_3

56 (R3). The former is a daytime Cl radical precursor affecting both marine and continental

57 environments and influencing next-day O_3 production.[17–20] NO_3 can also be directly taken up

58 onto aerosol (R4).

$$NO_2 + O_3 \rightarrow NO_3 \qquad \text{(R1)}$$
$$NO_3 + NO_2 \rightleftharpoons N_2O_5 \qquad \text{(R2)}$$
$$N_2O_{5\,(g)} + aerosol \rightarrow \phi ClNO_2 + (2 - \phi)HNO_3 \qquad \text{(R3)}$$
$$NO_3 + aerosol \rightarrow Products \qquad \text{(R4)}$$
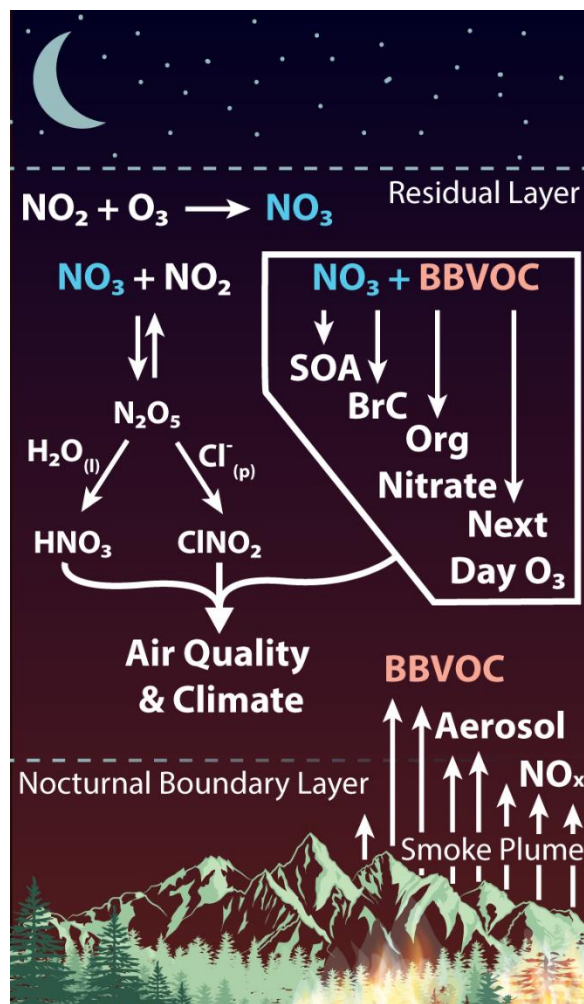
Figure 1. Schematic of nighttime NO_3 and N_2O_5 chemical processing in a biomass burning plume.

Mixing of background or smoke-derived[14] O_3 with NO_x in a BB plume leads to the production of NO_3, which may be rapid (>0.5 ppbv hr^{-1}). Recent laboratory measurements conducted during both the Fire Lab at Missoula Experiment (FLAME-4) and the on-going Fire Influence on Regional and Global Environments Experiment (FIREX) have provided detailed identification and quantification of emissions for a range of BBVOCs.[4,5,21–23] Emissions inventories from these experiments indicate that the compounds emitted and their relative concentrations depend on the fuel type (e.g., pine vs. grass), combustion process (e.g., smoldering or flaming), ignition

69   procedure (fast or slow), and pyrolysis temperature (e.g., high or low).[4,21,24,25] Generally, primary

70   BBVOC emissions include oxygenated hydrocarbons and aromatics (e.g., phenols), as well as

71   unsaturated hydrocarbons, biogenic and hetero-aromatic species.[4,5,21] Many such compounds are

72   very reactive toward NO_3[26–33] and may significantly limit its lifetime, promote secondary

73   organic aerosol formation (SOA)[34,35], and alter nighttime oxidative budgets.

74   The co-emission of NO_x, highly reactive VOCs, and aerosol particles leads to the potential for

75   significant nighttime chemical transformations. Despite this potential, there has been only one

76   aircraft campaign to date from which sampling of nighttime biomass burning plumes has been

77   reported.[36,37] The Southeast Nexus (SENEX) campaign in 2013 included 20 research flights of an

78   instrumented NOAA WP-3D aircraft and one of the goals was to study the interactions between

79   anthropogenic and biogenic emissions.[38] A night flight on July 2-3 targeted the emissions and

80   nighttime chemistry from a power plant plume near the Mississippi river. During this flight the

81   WP-3D also targeted and intercepted agricultural BB plumes yielding the first airborne study of

82   nighttime smoke that included NO_3 and N_2O_5 measurements.[36] Even so there has been no

83   previous analysis of BB NO_3 chemistry using nighttime aircraft intercepts.

84   Here, we present the first analysis of nighttime smoke oxidation based on aircraft intercepts of

85   fire plumes using data from this flight. With these observations we initiate a detailed chemical

86   box model to understand the chemical evolution of oxidants (NO_3, N_2O_5, O_3, and OH) and

87   BBVOCs over one night (10 hours) using emissions for rice straw to model a generic agricultural

88   burning plume. We then use this analysis to model nighttime chemistry in western wildfires

89   using emissions for a ponderosa pine fire.

90   **Field and Laboratory Measurements**

91   Field data for this study were taken from multiple instruments deployed on the NOAA WP-3D

92   aircraft during the SENEX 2013[38] flight on July 2-3, 2013 (20:00-03:00 CDT). Our analysis

93   utilizes data from the NOAA nitrogen oxide cavity ring-down spectrometer (CRDS) for NO_2,

94   NO_3, N_2O_5, and O_3,[39–42] as well as the NO_yO_3 chemiluminescence instrument (CL) for NO, NO_2,

95   O_3, and NO_y[43] with 1 Hz acquisition resolution. Within the plume regions we study, the

96   measurements of NO_2 and O_3 from the CRDS and CL instruments agree within 7%. We also use

97   data from an ultra-high sensitivity aerosol spectrometer (UHSAS) for aerosol size measurements

98   (1Hz) [44,45] and a proton-transfer-reaction mass spectrometer (PTR-MS) for VOC measurements

99   (1 s every 17 s)[46].

100   BB intercepts were identified by the enhancement above background of four species: black

101   carbon (BC), glyoxal (CHOCHO), CO, and acryloyl peroxynitrate (APAN).[36,47] BB identifier

102   data were provided by the NOAA airborne cavity enhanced spectrometer (ACES)[48] for glyoxal,

103   iodide chemical ionization mass spectrometer (I⁻ CIMS) for APAN[49], single particle soot

104   photometer (SP2) for black carbon[50], and vacuum ultra-violet fluorimeter for CO[51]. Power plant

105   plumes were identified by above background enhancements of NO_x and N_2O_5. While CO is also

106   present in the power plant plumes, the three other BB identifiers were not. Information on

107   background and plume measurements are in the SI (Table S1 & S2).

108   Five VOCs (toluene, isoprene + furan, methylvinylketone + methacrolein (MVK+MACR), and

109   methylethylketone (MEK)) as well as acetonitrile were measured by the PTR-MS during SENEX

110   and overlap with our inventory. However, we explain in the SI that we do not use these

111   observations because we do not know the fire source, number of fires, or fuel and plume age

112   estimates are highly uncertain (Figure S5).

113   Our detailed chemical box model uses emission inventories from Hatch et al.[5] and Koss et al.[4]

114   for the ponderosa pine and rice straw fuels. The BBVOC emissions from Hatch et al.[5,21] were

115   measured during FLAME-4 using the following instruments: two-dimensional gas

116   chromatography–time-of-flight mass spectrometry, open-path Fourier-transform infrared

117   spectroscopy[22], whole-air sampling with one-dimensional gas chromatography–mass

118   spectrometry, and PTR time-of-flight mass spectrometry (PTR-ToF)[52]. BBVOC emissions from

119   Koss et al.[4] were measured by PTR-ToF during FIREX. Details regarding how the two

120   inventories were merged is included in the SI. In general, for compounds shared between both

121   inventories, the emission ratios (E1) agree within an order of magnitude with some exceptions

122   (Figure S6). We propagate this variability into our model results (SI).

123   **Analysis and Modeling Methods**

124   We report our emissions in the form of laboratory-derived emission ratios (ER), which is the

125   background subtracted emitted compound (x) normalized to background subtracted CO.[4,21]

$$ER_x = \frac{x\ (ppbv)}{CO\ (ppmv)} \tag{E1}$$

126   These emissions are integrated over the entirety of the laboratory fires and therefore contain

127   emissions from all stages of the fire.

128   The modified combustion efficiency (MCE) was calculated for each plume.

$$MCE = \frac{CO_2 - CO_{2\,bkg}}{\left(CO_2 - CO_{2\,bkg}\right) + (CO - CO_{bkg})} \tag{E2}$$

129   During plume intercepts, the average MCE was $95 \pm 6\%$, which is consistent with previous

130   MCE calculations of the July 2/3 night flight.[36]

131   Total NO_3 reactivity toward BBVOCs is given by

$$k_{NO_3}^{BBVOC} = \sum k_{NO_3+BBVOC_i}[BBVOC_i] \qquad \text{(E3)}$$

132   where $k_{NO_3+BBVOC_i}$ is the bimolecular rate coefficient for $NO_3 + BBVOC_i$ and $k_{NO_3}^{BBVOC}$ is the

133   pseudo-first order rate coefficient. The bimolecular rate coefficients for NO_3, O_3, or OH +

134   BBVOC were taken from literature where available and estimated by structure activity

135   relationships[31,53] or structural similarity where unavailable (SI).

136   Due to limited literature on $NO_3 + BBVOC$ rate coefficients, our inventory excludes many

137   nitriles, amines, alkynes, acids, and other compounds whose rate coefficients were unavailable

138   and could not be estimated. We also removed saturated hydrocarbons because they are generally

139   unreactive toward NO_3.[28] Despite this, our merged inventory retains about 87% of the total

140   inventory carbon mass, or 96% by mass, with 235 compounds from Hatch et al.[5] and 171

141   compounds from Koss et al.[4] with 103 compounds shared in both inventories for a total of 303

142   unique compounds.

143   To calculate the observed NO_3 reactivity during SENEX BB plume intercepts we determined

144   BBVOC concentration using background corrected CO measured on the WP-3D.

$$BBVOC \; (ppbv) = ER_{BBVOC}(CO - CO_{bkg}) \qquad \text{(E4)}$$

145   As shown below, BBVOC is likely the main sink of NO_3; therefore, the extent of BBVOC

146   oxidation by NO_3 will be limited by the NO_x/BBVOC ratio as NO_x is the source for NO_3 (R1).

147   Furthermore, the relative oxidative importance between O_3 and NO_3 depends on the

148   NO_x/BBVOC ratio as explained by Edwards et al.[54] Therefore, in contrast to the method used for

149   calculating BBVOC concentration in SENEX fire plume intercepts described above, we initiate

150   our box model with fire emissions scaled to NO_x in order to preserve the NO_x/VOC ratio

151   observed during the fire lab experiments.

152   To estimate the emitted NO_x at the fire source we assume that the total reactive nitrogen (NO_y,

153   which does not include NH_3) is equivalent to the emitted NO_x. The NO_x/NO_y ratio as measured

154   during SENEX fire plume intercepts in Figure 2 was 0.84. We calculated the observed NO_y

155   emission ratio using NO_y (13.2 $\pm$ 3.1 ppbv) and CO (543.4 $\pm$ 87.7 ppbv) enhancements above

156   background. The calculated NO_y emission ratio, which we assume to be the NO_x emission ratio

157   at the fire source, was determined to be 24.3 $\pm$ 6.4 ppbv NO_y/ppmv CO for the plume intercept.

158   We compared the estimated observed NO_x emission ratio to the NO_x emission ratios reported by

159   Selimovic et al. for rice straw (43.9 ppbv NO_x/ppmv CO) and ponderosa pine (26.9$\pm$4.3 ppbv

160   NO_x/ppmv CO).[23] We then scaled the BBVOC emissions by this ratio (E5), effectively scaling

161   the fire emissions to the NO_x of the observed fire plume.

$$[BBVOC]^{model} = [BBVOC]^{inventory} * \frac{ER_{NO_y}^{observed}}{ER_{NO_x}^{inventory}} \tag{E5}$$

162   The NO_x emission ratio observed during the SENEX fire plume intercepts in Figure 2 was 45%

163   and 11% lower than the laboratory-derived NO_x emission ratio for rice straw and ponderosa pine

164   fires respectively. To correctly model the NO_3 oxidation of these fires we reduced our BBVOC

165   emissions by a factor of 55% for rice straw and 89% for ponderosa pine.

166   Model background and initial concentrations of NO_x, CO, and O_3 were taken from the SENEX

167   observations shown in Figure 2. We estimate the NO/NO_2 ratio at the fire source using the NO

168   and NO_2 emission ratios from FIREX for each fuel. The NO/NO_2 ratios used are 5.3 and 2.8 for

169   rice straw and ponderosa pine, respectively.[23] The background NO_2 mixing ratio was taken to be

170   0.9 ppbv. The background O_3 mixing ratio, 43.9 ppbv, was used as the starting O_3 mixing ratio

171   and is representative of the background O_3 in the region where BB plumes were intercepted

172   (Figure S3).

173   Box modeling was performed using the Framework for 0-D Atmospheric Modeling (F0AM)[55]

174   to investigate the evolution of oxidized mass and oxidant fractions over 10 hours (the

175   approximate duration of one night in July in the Southeastern U.S.). Chemical mechanisms were

176   adopted from the MCM (v3.3.1[56–60], via website: http://mcm.york.ac.uk) and published

177   mechanisms for methylguaiacol, syringol, o-guaiacol, and 3-methylfuran were added (Table

178   S4).[61–63] Compounds not included in the above references were modeled as a one-step reaction of

179   BBVOC + NO_3, BBVOC + O_3, or BBVOC + OH to form a single oxidation product.

180   All models were run at 298 K, typical experimental conditions for most published rate

181   coefficients. Temperatures during flight ranged between 288-290 K (SI). In order to account for

182   dilution processes, as well as entrainment of O_3, we apply a first order dilution of $k_{dil} = 1.16*10^{-5}$

183   s^{-1}, or a 24 hour lifetime. The sensitivity of this assumption is shown in Figure S2 and discussed

184   in the SI. We report a base case model result with upper and lower bound uncertainties based on

185   the emission and rate coefficient uncertainties. Although, as discussed in the SI, the bounds do

186   not provide information on the error distribution.

187   **Results and Discussion**

188   In panel A of Figure 2 the power plant plume intercepts (blue background) are distinguished

189   from the fire plume intercepts (red background) by CO, black carbon, APAN, and glyoxal.

190   Intercepts shown in Figure 2 were at an altitude between 700-900 meters. Relative to the BB

191   plume intercepts, the power plant plume intercepts exhibited elevated levels of NO_3 and N_2O_5

192   (Figure 2B). Figure 3A shows a flight map of the July 2-3 flight colored red during BB plume

193   intercepts and sized by the APAN mixing ratio. Roughly 97% of the indicated BB plumes do not

194   show signs of power plant plume mixing (SI). Green dashed boxes indicate sections of data

195   shown in Figure 2.

196   The flight covered the intersection of Missouri, Kentucky, Tennessee, and Arkansas at the

197   Mississippi river. According to the USDA CropScape database, this land is mainly agricultural

198   and therefore the fire plume is most likely the result of burning crop residue and stubble.[36,64]

199   Plume intercepts occurred near winter wheat crops, and rice straw crops are situated roughly 70

200   km northwest. Still, rice straw is the best available fuel proxy for agricultural burning emissions.

201   The wind direction was roughly northwesterly with most BB plume intercepts occurring in the

202   northwest corner of Tennessee.
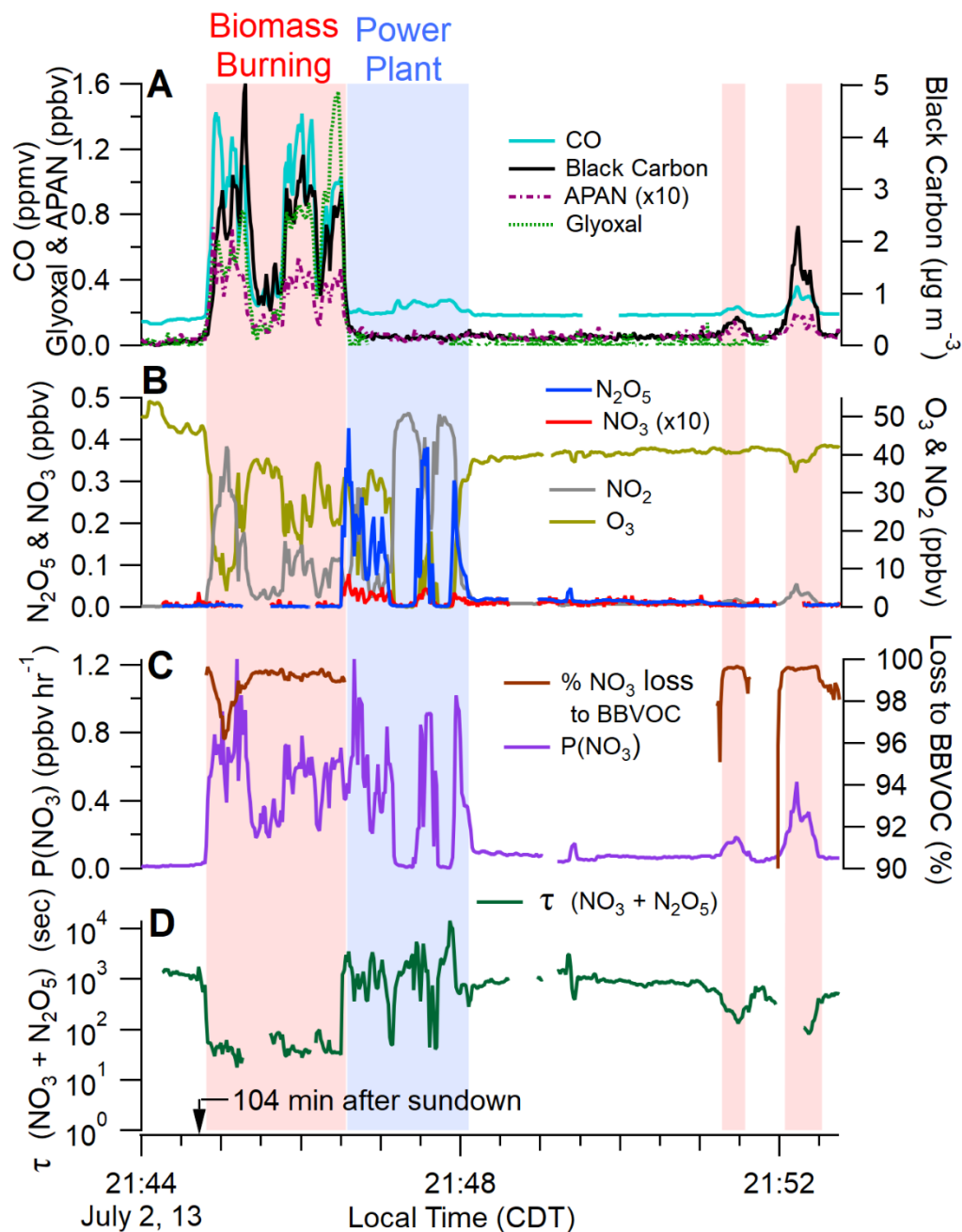
Figure 2. Time traces during representative sections of BB (red) and power plant (blue) plume intercepts made 104 minutes after sundown (SZA=90°). A: BB tracers, B: NO_3 N_2O_5, NO_2, and O_3 mixing ratio, C: production rate of NO_3 and the percentage of NO_3 reactivity toward BBVOCs, D: lifetime of NO_3 and N_2O_5.
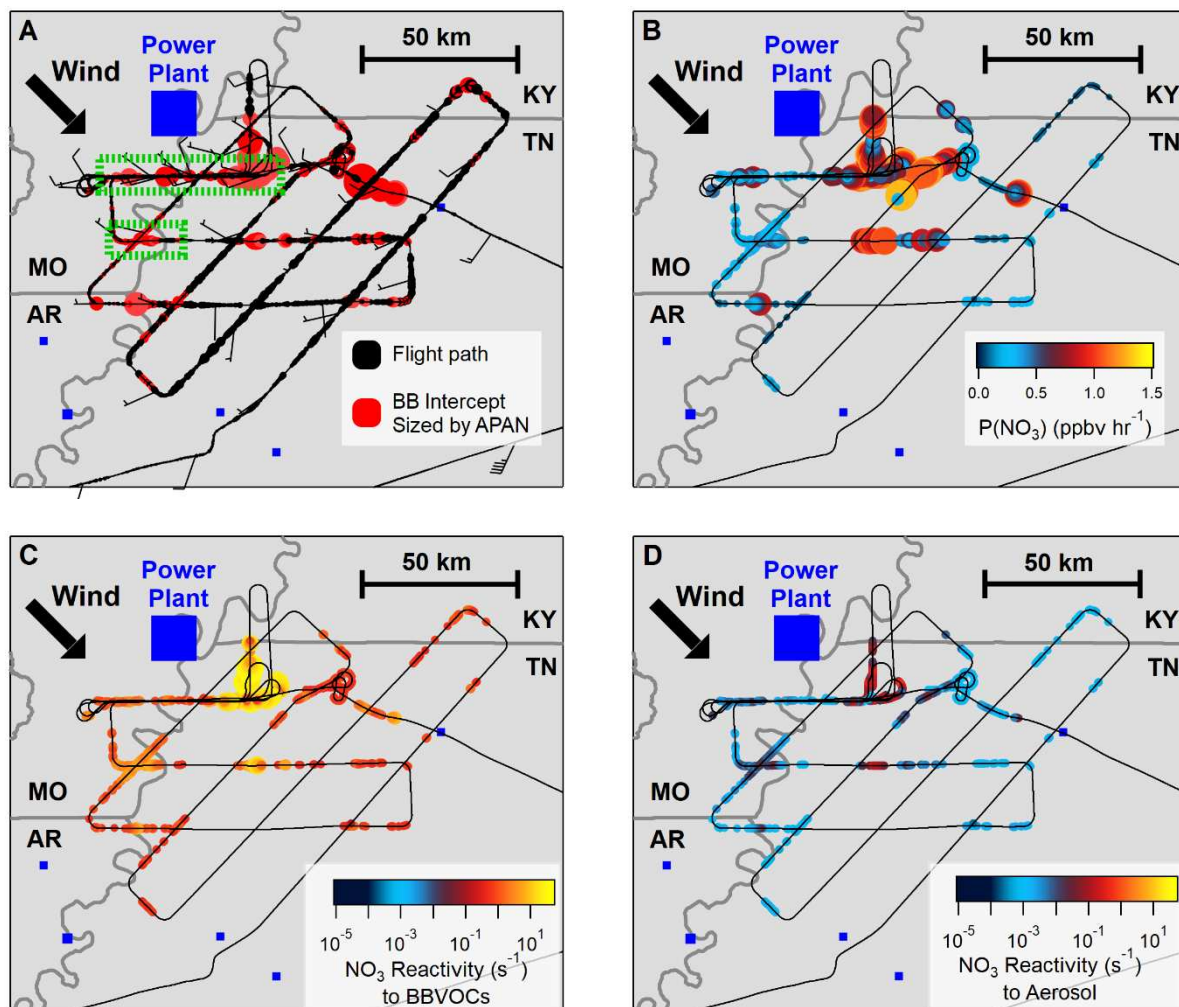
Figure 3. Flight maps of the SENEX July 2-3 2013 night flight. A: BB intercepts colored by red markers, sized by APAN (0.01-0.1 ppbv), and green dashes indicate sections shown in Figure 2, B: Production rate of NO_3, C: and D: are comparisons of NO_3 reactivity toward BBVOCs (C) and toward aerosol (D) on the same color and log scale.

To illustrate the NO_3 chemistry within a BB plume, we use previously published NO_3 and N_2O_5 analysis metrics. The NO_3 production rate, $P(NO_3)$, is the instantaneous source of NO_3 from the reaction of NO_2 with O_3 and is given in (E6).[15] The NO_3 + N_2O_5 lifetime (τ) is the ratio of NO_3 and N_2O_5 concentration to the NO_3 production rate (E7).[65] The summed lifetime is useful

216   because NO_3 and N_2O_5 reach an equilibrium state that is typically more rapid than the individual

217   sink reactions for either, such that they can be regarded as a sum.

$$P(NO_3) = k_{NO_3}[NO_2][O_3] \tag{E6}$$

$$\tau(NO_3 + N_2O_5) = \frac{NO_3 + N_2O_5}{P(NO_3)} \tag{E7}$$

218   P(NO_3) was large and of similar magnitude in both the power plant plume and BB plume

219   (Figure 2C). Figure 3B is colored by NO_3 production during BB intercepts only, and shows that

220   large NO_3 production rates, near 1 ppbv hr^{-1}, were observed during multiple BB plume

221   intercepts. Despite the large NO_3 radical production, the NO_3 and N_2O_5 concentrations within the

222   BB plume were below the 3 pptv[38] stated detection limit of the instrument (Figure 2B), yielding

223   short NO_3 + N_2O_5 lifetimes. Indeed, as shown in Figure 2D, τ is roughly a factor of 100 lower

224   within the BB plume as compared to the power plant plume and background air. Because the

225   NO_3 and N_2O_5 were below stated detection limits in the BB plumes, the corresponding lifetimes

226   shown in Figure 2D are upper limits, and the actual lifetimes may be considerably shorter.

227   The high production rate and short lifetime of NO_3 + N_2O_5 within the BB plume is evidence

228   for rapid NO_3 or N_2O_5 loss pathways. BB plumes contain large quantities of both aerosol and

229   BBVOCs, which provide two efficient NO_3/N_2O_5 loss pathways. To understand the competition

230   between these loss processes we calculated an instantaneous NO_3 reactivity toward aerosol and

231   toward BBVOCs. The total NO_3 loss to BBVOC is calculated using the sum of BBVOC

232   reactivity normalized to CO (E3). The total NO_3 loss to aerosol uptake is given as the sum of

233   both NO_3 and N_2O_5 uptake rate coefficients. By assuming steady state[66] for both NO_3 and N_2O_5,

234   we estimate the total aerosol uptake, and therefore NO_3 reactivity toward aerosol, as

$$k_{NO_3}^{aerosol} = K_{eq}[NO_2]k_{N_2O_5+aerosol} + k_{NO_3+aerosol} \tag{E8}$$

235   where $k_{NO_3}^{aerosol}$ is a first order rate coefficient, K_{eq} is the equilibrium constant between NO_3 and

236   N_2O_5 (R2), and $k_{x+aerosol}$ is the first order rate coefficient for N_2O_5 or NO_3 aerosol uptake

237   expressed below.

$$k_{x+aerosol} = \frac{\gamma \cdot \bar{c} \cdot SA}{4} \hspace{3cm} \text{(E9)}$$

238   Here, γ is the aerosol uptake coefficient, $\bar{c}$ is the mean molecular speed, and SA is the aerosol

239   surface area. Calculations use uptake coefficients of $\gamma_{N_2O_5} = 10^{-2}$ for N_2O_5[19] and $\gamma_{NO_3} = 10^{-3}$

240   for NO_3. However, γ_{NO_3} values have a wide range therefore we include calculations with $\gamma_{NO_3} =$

241   1 in the SI, but find similar results.[15]

242   Figure 3C & D compare the NO_3 reactivity toward BBVOCs, and aerosol uptake during BB

243   plume intercepts, respectively. In all BB intercepts, the calculated NO_3 reactivity toward

244   BBVOCs is a factor of 100 - 1000 greater than aerosol uptake. Figure 2C shows the percentage

245   of NO_3 reactivity dominated by BBVOC with a median >99%.

246   To understand which BBVOCs may be responsible for the rapid initial loss of NO_3 we

247   calculated the relative NO_3 reactivity for 303 compounds in rice straw and ponderosa pine

248   burning emissions. The top panel of Figure 4 shows the ranked order of the compounds that

249   account for 99% of the rice straw initial NO_3 reactivity. Eight furan or phenol compounds are

250   responsible for 75% of the initial NO_3 reactivity. Most of, the initial NO_3 reactivity for a rice

251   straw fire is accounted for by phenols ($60^{+20}_{-14}\%$) and furans ($23^{+20}_{-6}\%$), as well as pyrroles and

252   furfurals ($8^{+9}_{-3}\%$ combined).

253

254
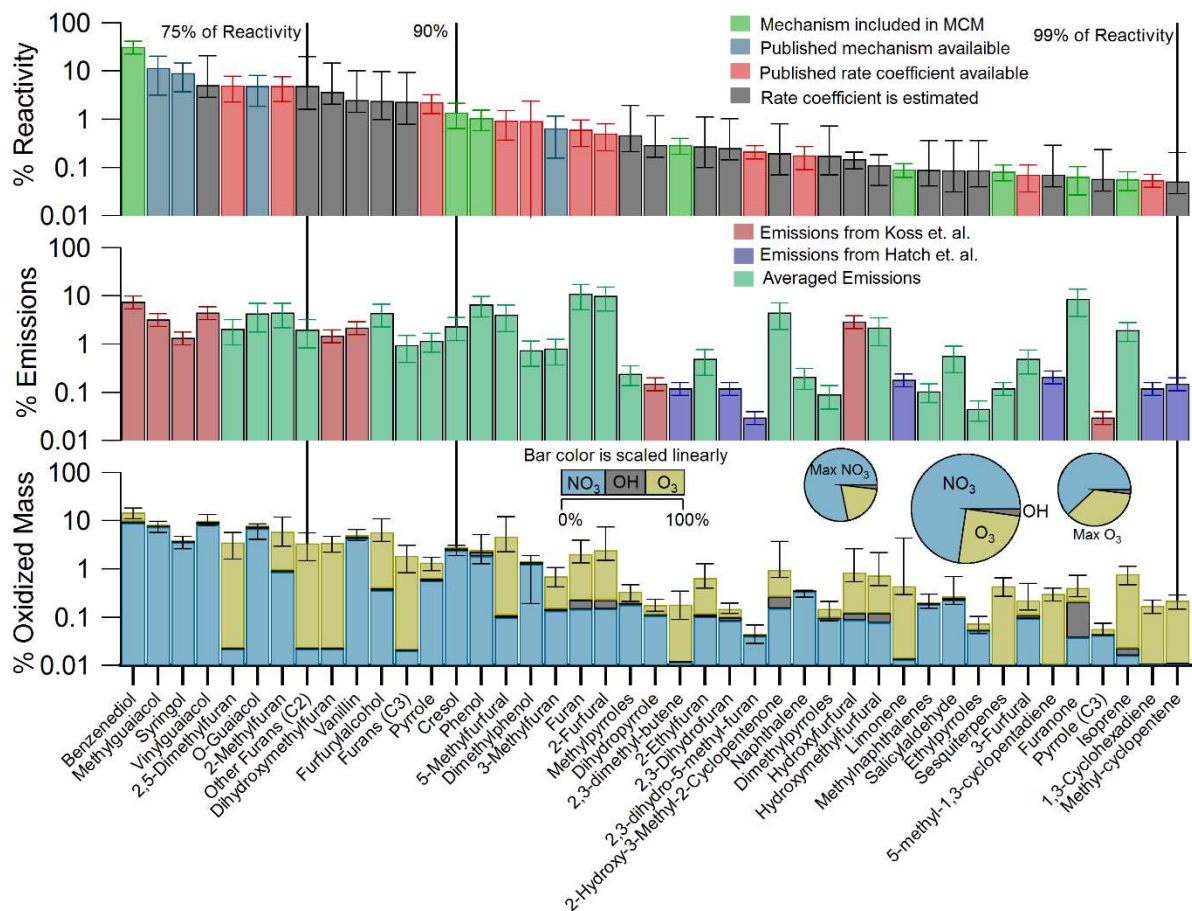
Figure 4. Rice Straw fuel. The top panel shows the ranked order of the compounds that account

for 99% of the rice straw initial NO_3 reactivity. The color scale describes the origin of the

mechanisms or rate coefficient used. The middle panel is the relative BBVOC emission ratio

normalized to the total BBVOC emission ratio and the color scale describes the origin of the

emissions data. The bottom panel is the relative nighttime reacted mass (10 hours) normalized to
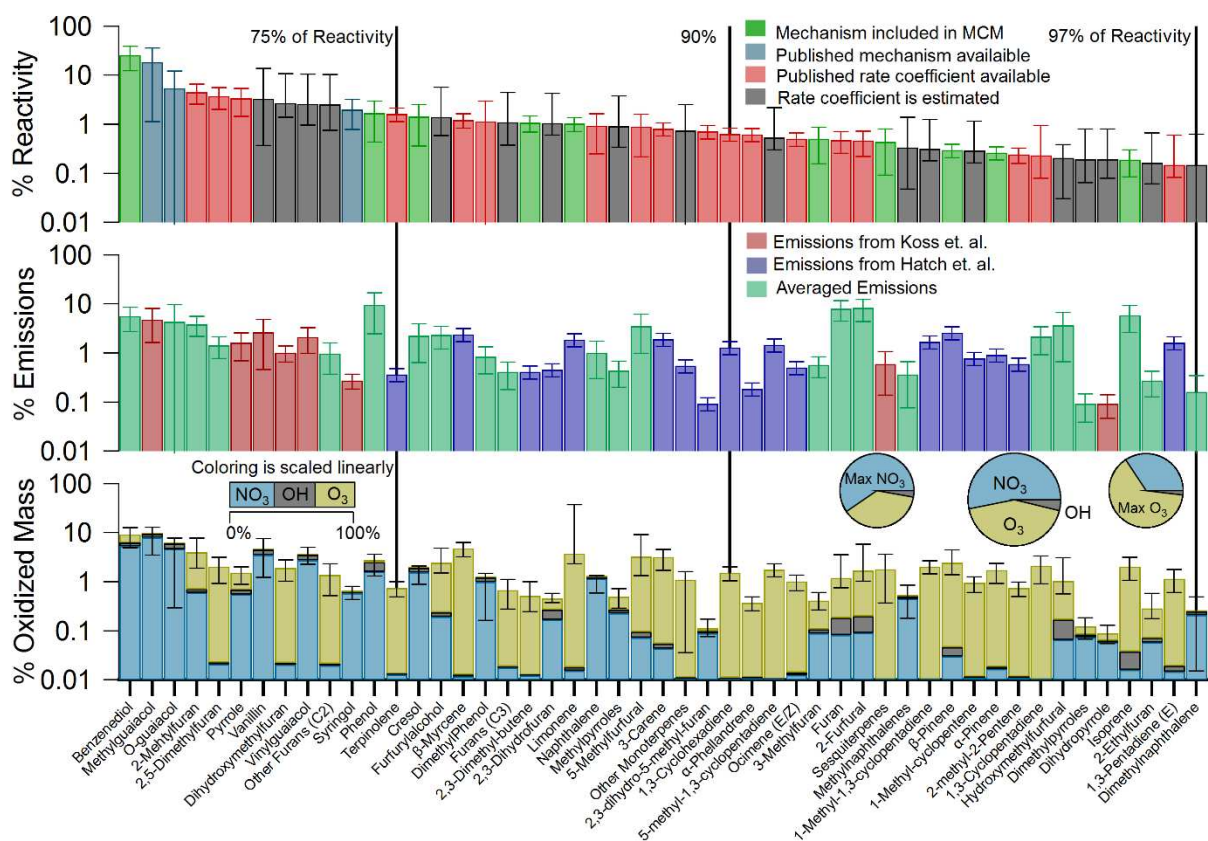
total reacted mass. While the bar height is on a log scale, the color scale is linear and indicates

the fraction of oxidation by NO_3 (blue), O_3 (gold), and OH (grey). The center pie chart shows the

fraction of reacted mass in the base case with the maximum NO_3 oxidation case to the left, and

maximum O_3 oxidation case to the right. All panels sum to 100%.

264 The top panel of Figure 5 shows the ranked order of the compounds that account for 97% of

265 the ponderosa pine initial NO_3 reactivity. The top 75% of initial NO_3 reactivity is distributed

266 among 13 compounds with phenols ($62_{-23}^{+27}\%$), furans ($18_{-4}^{+12}\%$), pyrrole and furfural ($8_{-3}^{+8}\%$

267 combined) again dominating the total reactivity. Unlike rice straw, a ponderosa pine fire plume

268 has significant reactivity towards terpenes ($8_{-1}^{+2}\%$). The initial NO_3 reactivity towards terpenes

269 and unsaturated hydrocarbons in a rice straw plume is <1%. These differences in reactivity are

270 due to differences in emissions between the two fuels as explained below.[5]

271

272 **Figure 5.** Same as Figure 4, but for the ponderosa pine fuel. In the bottom panel the bar height is

273 on a log scale, but the color scale is linear and indicates the fraction of oxidation by NO_3 (blue),

274 O_3 (gold), and OH (grey).

275   The middle panels of Figures 4 and 5 show the emission ratios for each compound normalized

276   to total emissions. The color indicates the origin of the emission ratio. The rice straw fire

277   emissions for compounds included in Figure 4 are mainly furans ($33\pm8\%$), phenols ($27\pm4\%$),

278   and furfurals ($24\pm6\%$), while unsaturated hydrocarbon and terpene emissions account for only

279    $3\pm1\%$. In contrast, the ponderosa pine fire emissions have a larger representation of terpenes

280   ($18\pm4\%$) and unsaturated hydrocarbons ($10\pm2\%$), but phenols ($33\pm10\%$), furans ($17\pm4\%$) and

281   furfurals ($18\pm6\%$) are all still significant.

282   To better understand smoke plume evolution and to determine the amount of BBVOC mass

283   oxidized during one night (10 hours), we ran a 0-D box model for both rice straw and ponderosa

284   pine fire emissions. NO_3 and N_2O_5 remained below 3 pptv (Figure S1), consistent with field

285   observations (Figure 2B). Figure S1 illustrates that the summed concentrations of the most

286   reactive BBVOCs are comparable to NO_2, suggesting there is approximately as much NO_3

287   precursor available as there is BBVOC to be oxidized. For both fuels, roughly 50-60% of NO_2

288   and the BBVOC compounds listed in Figure 4 and Figure 5 are depleted by chemistry (excluding

289   dilution) in one night. Our box-model suggests several abundant BBVOCs survive the night with

290   more than 50% of their initial starting concentration, such as phenol, furan, furfural and

291   hydroxymethylfurfural (SI).

292   HNO_3 production is complex within the model, and both maximum and minimum uncertainty

293   bounds on HNO_3 concentrations are the result of higher bound BBVOC emissions, but lower and

294   higher bound BBVOC rate coefficients, respectively. HNO_3 is the product of reactions of

295   phenolic compounds with NO_3, which proceeds by H-abstraction. HNO_3 production is

296   dominated by catechol + NO_3 (~60%) within the first few hours, but as the more reactive

297   compounds are depleted, the lesser reactive compounds like methyl guaiacol, guaiacol and

298   syringol react with NO_3 and dominate in the last two hours. HNO_3 may be lost to the particle

299   phase with concurrent NH_3 emission or other nitrogen species, however this loss mechanism is

300   not included in our model.

301   For both fuels, catechol is the most reactive compound, and accounts for $32\pm9\%$ and $26\pm13\%$

302   of initial NO_3 reactivity at the start of the simulation for rice straw and ponderosa pine plumes,

303   respectively. However, Koss et al.[4] were unable to distinguish between catechol and

304   methylfurfural at m/z = 110.1 We assume a 50/50 contribution here, which yields catechol

305   emission ratios of 2.5 ± 0.8 ppbv ppmv^{-1} CO for rice straw and 1.5 ± 0.6 ppbv ppmv^{-1} CO for

306   ponderosa pine. Still, the high reactivity is mainly due to the large catechol rate coefficient

307   $(9.9*10^{-11}$ cm^3 molecule^{-1} s$^{-1})$[67], which is the third greatest among the emitted compounds.

308   Catechol is known to react with NO_3 by H-abstraction, with subsequent addition of NO_2 to the

309   aromatic peroxy radical to form 4-nitrocatechol with a near-unity molar yield of 0.91 ± 0.06.[68]

310   Further, 4-nitrocatechol is expected to almost completely (96%) partition to the particle phase.[68]

311   Recently, Hartikainen et al.[25] investigated dark oxidation of residential wood combustion and

312   found strong correlations between the depletion of phenolic compounds and the formation of

313   NO_3-initiated SOA. In wintertime BB events, 4-nitrocatechol and other derivatives have been

314   detected in aerosol and are considered important light-absorbing components of brown carbon

315   (BrC).[35,69–76]

316   SOA yields are a function of mass loadings.[77] Using a catechol mass loading of 300 μg m^{-3}

317   from Finewax et al.[68] as well as a total observed aerosol plume measurement of 58.7 μg m^{-3} we

318   estimate a 4-nitrocatechol SOA mass yield of 120%. Assuming 0.6 ppbv of catechol in

319   ponderosa pine and 0.8 ppbv in rice straw (initial model conditions) with 44 ppbv O_3, 13 ppbv of

320   NO_x and $k_{dil} = 1.16*10^{-5}$ s^{-1}, we estimate the SOA produced from catechol to be 3.8 ± 1.0 μg m^{-3}

321   in 8 hours and $4.0^{+1.1}_{-1.0}$ μg m^{-3} in 8.5 hours for a rice straw and ponderosa pine plume,

322   respectively. Further, there is evidence to suggest furans and furfurals may also be a source of

323   SOA precursors.[5,25]

324   The bottom panel of Figure 4 shows the reacted mass per compound normalized to the total

325   reacted mass. The bar height is on a log scale, but the bar color is linearly scaled and indicates

326   the fraction of nighttime oxidation by NO_3 (blue), O_3 (gold), and OH (grey) after 10 hours for

327   each compound. The center pie chart in Figure 4 and 5 represents the base case fraction of

328   reactant mass oxidized by each oxidant. The left and right pie charts show results for the

329   estimated maximum possible NO_3 and maximum possible O_3 oxidation, respectively.

330   Uncertainty in the fraction of oxidized mass is calculated from the uncertainties in individual

331   compound emissions and rate coefficients. For the compounds comprising a rice straw BB

332   plume, the majority of mass is oxidized by NO_3 (72^{+6}_{-11}%). This is expected because the rice

333   straw fuel emissions are rich in oxygenated aromatic and hetero-aromatic emissions, which are

334   generally less reactive toward O_3. Terpenes and unsaturated hydrocarbons, which are a small

335   fraction of emissions in Figure 4, are relatively more reactive toward O_3. Even so, O_3 still has a

336   significant oxidative impact and is responsible for 26^{+11}_{-6}% of oxidized BBVOC mass.

337   The relative amount of oxidized mass for ponderosa pine is shown in the bottom panel of

338   Figure 5. Almost half of the oxidized mass for compounds included in Figure 5 is due to O_3

339   (43^{+21}_{-6}%) for our base case. The phenolic compounds mainly undergo NO_3 oxidation while

340   terpenes and unsaturated hydrocarbons are mainly oxidized by O_3. Furans and the hetero-

341   aromatics are oxidized approximately evenly by O_3 and NO_3. The increased fraction of O_3

342   oxidation is the result of the increased fraction of unsaturated hydrocarbon and terpenes in the

343   ponderosa pine emissions when compared to rice straw.

344   The nighttime chemical evolution and oxidation products of a biomass burning plume will

345   depend on the relative NO_3 and O_3 reactivity. Neglecting the small contribution from OH

346   oxidation, Edwards et al.[54] show the competition between NO_3 and O_3 oxidation of biogenic

347   VOCs (BVOC) is dependent on the NO_x/BVOC ratio. We scaled our BBVOC emissions to

348   maintain the NO_x/BBVOC ratio expected for rice straw (0.4 ± 0.1) or ponderosa pine (0.3 ± 0.1)

349   emissions. However, because fires are highly variable, the NO_x/BBVOC ratio for any given fuel

350   may vary from fire to fire. For rice straw, a factor of two increase in NO_x increases the fraction

351   of NO_3 oxidation from 72% to 84%, while a factor of two decrease in NO_x decreases relative

352   NO_3 oxidation to 55%. Similarly, for ponderosa pine, doubling NO_x increases the fraction of NO_3

353   oxidation from 53% to 66%, while halving NO_x decreases relative NO_3 oxidation to 37% and

354   increases O_3 to 57%. Furthermore, we find that a factor of two change in ambient O_3

355   concentration has little effect on the relative NO_3 and O_3 reactivity (see SI).

356   Our reactivity calculations and box-model results are most limited by a lack of kinetic and

357   mechanistic studies for O_3, NO_3, and OH + BBVOCs reactions. Kinetic and mechanistic studies

358   of furan, furfural, phenol, and pyrrole analogues reacting with NO_3 will be most critical to

359   understanding nighttime BB processes, which we highlight in the SI.

360   The time of day in which a fire is active will determine the fate of its emissions. This paper

361   presents the first nighttime aircraft intercepts of a BB plume combined with an inventory of 303

362   BBVOC emissions and an oxidation model to predict the lifetime and fate of BB emissions in the

363   dark. Fire emissions at times near sunset will undergo the chemistry we have detailed here,

364   which suggests a roughly 60% depletion (for both rice straw and ponderosa pine) of fire-derived

365   NO_x. We find that nighttime chemistry is likely to proceed by NO_3, rather than N_2O_5, further

366   slowing the loss of NO_x (R1 & R2). Our model applies to chemistry at the center of a plume and

367   does not include dispersion. Dispersion mixes NO_x with background O_3 at the edges of the plume

368   leading to faster depletion, and therefore the values we report are likely lower limits. Even so,

369   18-19% of BBVOC mass, out of the total BBVOC mass that we model, will be oxidized in one

370   night. That is roughly a 55% depletion of the BBVOCs that are reactive toward NO_3. There is

371   evidence that many of these NO_3 reactive compounds can form secondary BrC aerosol[35,69–76],

372   suggesting nighttime oxidation may be a significant source of BB derived BrC. Furthermore,

373   future BB photochemical models should consider that these reactive phenolic-, furan- and

374   furfural-like compounds are not only reactive toward NO_3, but also O_3 and OH, thus affecting

375   next-day BB photochemistry.

376   Acknowledgments

378   Supporting Information Available

379   Figure S1, box model time traces of key species, Figure S2, box model sensitivity to the dilution

380   rate coefficient, Figure S3, Correlation of O_3 and NO_2 from aircraft observations, Figure S4,

381   altitude profiles of key species and potential temperature, Figure S5, plume age estimates, Figure

382   S6, variability in emission ratios. Table S1, BB plume and background values, Table S2, Plumes

383   and background times, Table S3, List of reactions excluded from the MCM, Table S4,

384   mechanisms added to the MCM. This information is available free of charge via the Internet at

385   http://pubs.acs.org.

386   References

387   (1)   Dennison, P. E.; Brewer, S. C.; Arnold, J. D.; Moritz, M. A. Large Wildfire Trends in the

388   Western United States, 1984-2011. *Geophys. Res. Lett.* **2014**, *41*, 2014GL059576.

389   https://doi.org/10.1002/2014gl059576.

390   (2)   Westerling, A. L.; Hidalgo, H. G.; Cayan, D. R.; Swetnam, T. W. Warming and Earlier

391   Spring Increase Western U.S. Forest Wildfire Activity. *Science (80-.).* **2006**, *313* (5789),

392   940–943.

393   (3)   Pope, C. A.; Dockery, D. W. Health Effects of Fine Particulate Air Pollution: Lines That

394   Connect. *J. Air Waste Manag. Assoc.* **2006**, *56* (6), 709–742.

395   https://doi.org/10.1080/10473289.2006.10464485.

396   (4)   Koss, A. R.; Sekimoto, K.; Gilman, J. B.; Selimovic, V.; Coggon, M. M.; Zarzana, K. J.;

397   Yuan, B.; Lerner, B. M.; Brown, S. S.; Jimenez, J. L.; Krechmer, J.; Roberts, J. M.;

398   Warneke, C.; Yokelson, R. J.; de Gouw, J. Non-Methane Organic Gas Emissions from

399   Biomass Burning: Identification, Quantification, and Emission Factors from PTR-ToF

400   during the FIREX 2016 Laboratory Experiment. *Atmos. Chem. Phys.* **2018**, *18* (October),

401   3299–3319. https://doi.org/10.5194/acp-2017-924.

402   (5)   Hatch, L. E.; Yokelson, R. J.; Stockwell, C. E.; Veres, P. R.; Simpson, I. J.; Blake, D. R.;

403   Orlando, J. J.; Barsanti, K. C. Multi-Instrument Comparison and Compilation of Non-

404   Methane Organic Gas Emissions from Biomass Burning and Implications for Smoke-

405   Derived Secondary Organic Aerosol Precursors. *Atmos. Chem. Phys.* **2017**, *17* (2), 1471–

406   1489. https://doi.org/10.5194/acp-17-1471-2017.

407   (6)   Rotstayn, L. D.; Penner, J. E. Indirect Aerosol Forcing, Quasi Forcing, and Climate

408   Response. *J. Clim.* **2001**, *14* (13), 2960–2975. https://doi.org/10.1175/1520-

409   0442(2001)014<2960:IAFQFA>2.0.CO;2.

410   (7)   Andreae, M. O.; Merlet, P. Emission of Trace Gases and Aerosols from Biomass Burning.

411   *Global Biogeochem. Cycles* **2001**, *15* (4), 955–966.

412   https://doi.org/10.1029/2000GB001382.

413   (8)   Yokelson, R. J.; Crounse, J. D.; DeCarlo, P. F.; Karl, T.; Urbanski, S.; Atlas, E.; Campos,

414   T.; Shinozuka, Y.; Kapustin, V.; Clarke, A. D.; Weinheimer, A.; Knapp, D. J.; Montzka,

415   D. D.; Holloway, J.; Weibring, P.; Flocke, F.; Zheng, W.; Toohey, D.; Wennberg, P. O.;

416   Wiedinmyer, C.; Mauldin, L.; Fried, A.; Richter, D.; Walega, J.; Jimenez, J. L.; Adachi,

417   K.; Buseck, P. R.; Hall, S. R.; Shetter, R. Emissions from Biomass Burning in the

418   Yucatan. *Atmos. Chem. Phys.* **2009**, *9* (15), 5785–5812. https://doi.org/10.5194/acp-9-

419   5785-2009.

420   (9)   Hennigan, C. J.; Sullivan, A. P.; Collett, J. L.; Robinson, A. L. Levoglucosan Stability in

421   Biomass Burning Particles Exposed to Hydroxyl Radicals. *Geophys. Res. Lett.* **2010**, *37*

422   (9), 1–4. https://doi.org/10.1029/2010GL043088.

423   (10)   Hennigan, C. J.; Miracolo, M. A.; Engelhart, G. J.; May, A. A.; Presto, A. A.; Lee, T.;

424   Sullivan, A. P.; McMeeking, G. R.; Coe, H.; Wold, C. E.; Hao, W. M.; Gilman, J. B.;

425   Kuster, W. C.; De Gouw, J.; Schichtel, B. A.; Collett, J. L.; Kreidenweis, S. M.; Robinson,

426   A. L. Chemical and Physical Transformations of Organic Aerosol from the Photo-

427   Oxidation of Open Biomass Burning Emissions in an Environmental Chamber. *Atmos.*

428   *Chem. Phys.* **2011**, *11* (15), 7669–7686. https://doi.org/10.5194/acp-11-7669-2011.

429   (11)   Ortega, A. M.; Day, D. A.; Cubison, M. J.; Brune, W. H.; Bon, D.; De Gouw, J. A.;

430   Jimenez, J. L. Secondary Organic Aerosol Formation and Primary Organic Aerosol

431   Oxidation from Biomass-Burning Smoke in a Flow Reactor during FLAME-3. *Atmos.*

432   *Chem. Phys.* **2013**, *13* (22), 11551–11571. https://doi.org/10.5194/acp-13-11551-2013.

433   (12)   Bruns, E. A.; El Haddad, I.; Slowik, J. G.; Kilic, D.; Klein, F.; Baltensperger, U.; Prévôt,

434   A. S. H. Identification of Significant Precursor Gases of Secondary Organic Aerosols

435   from Residential Wood Combustion. *Sci. Rep.* **2016**, *6* (June), 1–9.

436   https://doi.org/10.1038/srep27881.

437   (13)   Bruns, E. A.; El Haddad, I.; Keller, A.; Klein, F.; Kumar, N. K.; Pieber, S. M.; Corbin, J.

438   C.; Slowik, J. G.; Brune, W. H.; Baltensperger, U.; Prévôt, A. S. H. Inter-Comparison of

439   Laboratory Smog Chamber and Flow Reactor Systems on Organic Aerosol Yield and

440   Composition. *Atmos. Meas. Tech.* **2015**, *8* (6), 2315–2332. https://doi.org/10.5194/amt-8-

441   2315-2015.

442   (14)   Jaffe, D. A.; Wigder, N. L. Ozone Production from Wildfires: A Critical Review. *Atmos.*

443   *Environ.* **2012**, *51*, 1–10. https://doi.org/http://dx.doi.org/10.1016/j.atmosenv.2011.11.063.

444   (15)   Brown, S. S.; Stutz, J. Nighttime Radical Observations and Chemistry. *Chem. Soc. Rev.*

445   **2012**, *41*, 6405–6447. https://doi.org/10.1039/c2cs35181a.

446   (16)   Wayne, R. .; Barnes, I.; Biggs, P.; Burrows, J. .; Canosa-Mas, C. .; Hjorth, J.; Le Bras, G.;

447   Moortgat, G. .; Perner, D.; Poulet, G.; Restelli, G.; Sidebottom, H. The Nitrate Radical:

448   Physics, Chemistry, and the Atmosphere. *Atmos. Environ. Part A. Gen. Top.* **1991**, *25* (1),

449   1–203. https://doi.org/10.1016/0960-1686(91)90192-A.

450   (17)   Osthoff, H. D.; Roberts, J. M.; Ravishankara, A. R.; Williams, E. J.; Lerner, B. M.;

451   Sommariva, R.; Bates, T. S.; Coffman, D.; Quinn, P. K.; Dibb, J. E.; Stark, H.;

452   Burkholder, J. B.; Talukdar, R. K.; Meagher, J.; Fehsenfeld, F. C.; Brown, S. S. High

453   Levels of Nitryl Chloride in the Polluted Subtropical Marine Boundary Layer. *Nat.*

454   *Geosci.* **2008**, *1* (5), 324–328. https://doi.org/10.1038/ngeo177.

455 (18) Thornton, J. A.; Kercher, J. P.; Riedel, T. P.; Wagner, N. L.; Cozic, J.; Holloway, J. S.;

456 Dubé, W. P.; Wolfe, G. M.; Quinn, P. K.; Middlebrook, A. M.; Alexander, B.; Brown, S.

457 S. A Large Atomic Chlorine Source Inferred from Mid-Continental Reactive Nitrogen

458 Chemistry. *Nature* **2010**, *464* (7286), 271–274. https://doi.org/10.1038/nature08905.

459 (19) Chang, W. L.; Bhave, P. V.; Brown, S. S.; Riemer, N.; Stutz, J.; Dabdub, D.

460 Heterogeneous Atmospheric Chemistry, Ambient Measurements, and Model Calculations

461 of N2O5: A Review. *Aerosol Sci. Technol.* **2011**, *45* (6), 655–685.

462 https://doi.org/10.1080/02786826.2010.551672.

463 (20) Ahern, A.; Goldberger, L.; Jahl, L.; Thornton, J.; Sullivan, R. C. Production of N2O5 and

464 ClNO2 through Nocturnal Processing of Biomass-Burning Aerosol. *Environ. Sci. Technol.*

465 **2018**, *52* (2), 550–559. https://doi.org/10.1021/acs.est.7b04386.

466 (21) Hatch, L. E.; Luo, W.; Pankow, J. F.; Yokelson, R. J.; Stockwell, C. E.; Barsanti, K. C.

467 Identification and Quantification of Gaseous Organic Compounds Emitted from Biomass

468 Burning Using Two-Dimensional Gas Chromatography–time-of-Flight Mass

469 Spectrometry. *Atmos. Chem. Phys.* **2015**, *15* (4), 1865–1899. https://doi.org/10.5194/acp-

470 15-1865-2015.

471 (22) Stockwell, C. E.; Yokelson, R. J.; Kreidenweis, S. M.; Robinson, A. L.; Demott, P. J.;

472 Sullivan, R. C.; Reardon, J.; Ryan, K. C.; Griffith, D. W. T.; Stevens, L. Trace Gas

473 Emissions from Combustion of Peat, Crop Residue, Domestic Biofuels, Grasses, and

474 Other Fuels: Configuration and Fourier Transform Infrared (FTIR) Component of the

475 Fourth Fire Lab at Missoula Experiment (FLAME-4). *Atmos. Chem. Phys.* **2014**, *14* (18),

476 9727–9754. https://doi.org/10.5194/acp-14-9727-2014.

477   (23)   Selimovic, V.; Yokelson, R. J.; Warneke, C.; Roberts, J. M.; de Gouw, J. A.; Griffith, D.

478   W. T. Aerosol Optical Properties and Trace Gas Emissions from Laboratory-Simulated

479   Western US Wildfires during FIREX. *Atmos. Chem. Phys.* **2017**, *18*, 2929–2948.

480   https://doi.org/10.5194/acp-18-2929-2018.

481   (24)   Sekimoto, K.; Koss, A. R.; Gilman, J. B.; Selimovic, V.; Coggon, M. M.; Zarzana, K. J.;

482   Yuan, B.; Lerner, B. M.; Brown, S. S.; Warneke, C.; Yokelson, R. J.; Roberts, J. M.; de

483   Gouw, J. High- and Low-Temperature Pyrolysis Profiles Describe Volatile Organic

484   Compound Emissions from Western US Wildfire Fuels. *Atmos. Chem. Phys. Discuss.*

485   **2018**, No. February, 1–39. https://doi.org/10.5194/acp-2018-52.

486   (25)   Hartikainen, A.; Yli-Pirilä, P.; Tiitta, P.; Leskinen, A.; Kortelainen, M.; Orasche, J.;

487   Schnelle-Kreis, J.; Lehtinen, K.; Zimmermann, R.; Jokiniemi, J.; Sippula, O. Volatile

488   Organic Compounds from Logwood Combustion: Emissions and Transformation under

489   Dark and Photochemical Aging Conditions in a Smog Chamber. *Environ. Sci. Technol.*

490   **2018**, *52* (4979–4988), acs.est.7b06269. https://doi.org/10.1021/acs.est.7b06269.

491   (26)   Atkinson, R.; Arey, J. Gas-Phase Tropospheric Chemistry of Biogenic Volatile Organic

492   Compounds: A Review. In *Atmospheric Environment*; Pergamon, 2003; Vol. 37, pp 197–

493   219. https://doi.org/10.1016/S1352-2310(03)00391-1.

494   (27)   Atkinson, R.; Arey, J. Atmospheric Degradation of Volatile Organic Compounds. *Chem.*

495   *Rev.* **2003**, *103* (3), 4605–4638. https://doi.org/10.1021/cr0206420.

496   (28)   Atkinson, R. Kinetics and Mechanisms of the Gas-Phase Reactions of the NO3 Radical

497   with Organic Compounds. *Journal of Physical and Chemical Reference Data*. 1991, pp

498   459–507. https://doi.org/10.1063/1.555887.

499   (29)   El Zein, A.; Coeur, C.; Obeid, E.; Lauraguais, A.; Fagniez, T. Reaction Kinetics of

500   Catechol (1,2-Benzenediol) and Guaiacol (2-Methoxyphenol) with Ozone. *J. Phys. Chem.*

501   *A* **2015**, *119* (26), 6759–6765. https://doi.org/10.1021/acs.jpca.5b00174.

502   (30)   Martínez, E.; Cabañas, B.; Aranda, A.; Martín, P.; Salgado, S. Absolute Rate Coefficients

503   for the Gas-Phase Reactions of NO3 Radical with a Series of Monoterpenes at T = 298 to

504   433 K. *J. Atmos. Chem.* **1999**, *33* (3), 265–282.

505   https://doi.org/10.1023/A:1006178530211.

506   (31)   Kerdouci, J.; Picquet-Varrault, B.; Doussin, J. F. Structure-Activity Relationship for the

507   Gas-Phase Reactions of NO3radical with Organic Compounds: Update and Extension to

508   Aldehydes. *Atmos. Environ.* **2014**, *84* (3), 363–372.

509   https://doi.org/10.1016/j.atmosenv.2013.11.024.

510   (32)   Grosjean, D.; Williams, E. L. Environmental Persistence of Organic Compounds

511   Estimated from Structure-Reactivity and Linear Free-Energy Relationships. Unsaturated

512   Aliphatics. *Atmos. Environ. Part A, Gen. Top.* **1992**, *26* (8), 1395–1405.

513   https://doi.org/10.1016/0960-1686(92)90124-4.

514   (33)   Cabañas, B.; Baeza, M. T.; Salgado, S.; Martín, P.; Taccone, R.; Martínez, E. Oxidation of

515   Heterocycles in the Atmosphere: Kinetic Study of Their Reactions with NO3 Radical. *J.*

516   *Phys. Chem. A* **2004**, *108* (49), 10818–10823. https://doi.org/10.1021/jp046524t.

517   (34)   Harrison, M. A. J.; Barra, S.; Borghesi, D.; Vione, D.; Arsene, C.; Iulian Olariu, R.

518   Nitrated Phenols in the Atmosphere: A Review. *Atmospheric Environment*. 2005, pp 231–

519   248. https://doi.org/10.1016/j.atmosenv.2004.09.044.

520   (35)   Laskin, A.; Laskin, J.; Nizkorodov, S. A. Chemistry of Atmospheric Brown Carbon.

521   *Chem. Rev.* **2015**, *115* (10), 4335–4382. https://doi.org/10.1021/cr5006167.

522   (36) Zarzana, K. J.; Min, K. E.; Washenfelder, R. A.; Kaiser, J.; Krawiec-Thayer, M.; Peischl,

523   J.; Neuman, J. A.; Nowak, J. B.; Wagner, N. L.; Dubè, W. P.; Clair, J. M. S.; Wolfe, G.

524   M.; Hanisco, T. F.; Keutsch, F. N.; Ryerson, T. B.; Brown, S. S. Emissions of Glyoxal and

525   Other Carbonyl Compounds from Agricultural Biomass Burning Plumes Sampled by

526   Aircraft. *Environ. Sci. Technol.* **2017**, *51* (20), 11761–11770.

527   https://doi.org/10.1021/acs.est.7b03517.

528   (37) Neuman, J. A.; Trainer, M.; Brown, S. S.; Min, K. E.; Nowak, J. B.; Parrish, D. D.;

529   Peischl, J.; Pollack, I. B.; Roberts, J. M.; Ryerson, T. B.; Veres, P. R. HONO Emission

530   and Production Determined from Airborne Measurements over the Southeast U.S. *J.*

531   *Geophys. Res.* **2016**, *121* (15), 9237–9250. https://doi.org/10.1002/2016JD025197.

532   (38) Warneke, C.; Trainer, M.; De Gouw, J. A.; Parrish, D. D.; Fahey, D. W.; Ravishankara, A.

533   R.; Middlebrook, A. M.; Brock, C. A.; Roberts, J. M.; Brown, S. S.; Neuman, J. A.;

534   Lerner, B. M.; Lack, D.; Law, D.; Hübler, G.; Pollack, I.; Sjostedt, S.; Ryerson, T. B.;

535   Gilman, J. B.; Liao, J.; Holloway, J.; Peischl, J.; Nowak, J. B.; Aikin, K. C.; Min, K. E.;

536   Washenfelder, R. A.; Graus, M. G.; Richardson, M.; Markovic, M. Z.; Wagner, N. L.;

537   Welti, A.; Veres, P. R.; Edwards, P.; Schwarz, J. P.; Gordon, T.; Dube, W. P.; McKeen, S.

538   A.; Brioude, J.; Ahmadov, R.; Bougiatioti, A.; Lin, J. J.; Nenes, A.; Wolfe, G. M.;

539   Hanisco, T. F.; Lee, B. H.; Lopez-Hilfiker, F. D.; Thornton, J. A.; Keutsch, F. N.; Kaiser,

540   J.; Mao, J.; Hatch, C. D. Instrumentation and Measurement Strategy for the NOAA

541   SENEX Aircraft Campaign as Part of the Southeast Atmosphere Study 2013. *Atmos.*

542   *Meas. Tech.* **2016**, *9* (7), 3063–3093. https://doi.org/10.5194/amt-9-3063-2016.

543   (39)   Brown, S. S.; Stark, H.; Ravishankara, A. R. Cavity Ring-down Spectroscopy for

544   Atmospheric Trace Gas Detection: Application to the Nitrate Radical (NO3). *Appl. Phys.*

545   *B Lasers Opt.* **2002**, *75* (2–3), 173–182. https://doi.org/10.1007/s00340-002-0980-y.

546   (40)   Dubé, W. P.; Brown, S. S.; Osthoff, H. D.; Nunley, M. R.; Ciciora, S. J.; Paris, M. W.;

547   McLaughlin, R. J.; Ravishankara, A. R. Aircraft Instrument for Simultaneous, *in Situ*

548   Measurement of NO3 and N2O5 via Pulsed Cavity Ring-down Spectroscopy. *Rev. Sci.*

549   *Instrum.* **2006**, *77* (3), 034101. https://doi.org/10.1063/1.2176058.

550   (41)   Fuchs, H.; Dubé, W. P.; Ciciora, S. J.; Brown, S. S. Determination of Inlet Transmission

551   and Conversion Efficiencies for in Situ Measurements of the Nocturnal Nitrogen Oxides,

552   NO3, N 2O5 and NO2, via Pulsed Cavity Ring-down Spectroscopy. *Anal. Chem.* **2008**, *80*

553   (15), 6010–6017. https://doi.org/10.1021/ac8007253.

554   (42)   Wild, R. J.; Edwards, P. M.; Dube, W. P.; Baumann, K.; Edgerton, E. S.; Quinn, P. K.;

555   Roberts, J. M.; Rollins, A. W.; Veres, P. R.; Warneke, C.; Williams, E. J.; Yuan, B.;

556   Brown, S. S.; Dubé, W. P.; Baumann, K.; Edgerton, E. S.; Quinn, P. K.; Roberts, J. M.;

557   Rollins, A. W.; Veres, P. R.; Warneke, C.; Williams, E. J.; Yuan, B.; Brown, S. S. A

558   Measurement of Total Reactive Nitrogen, NOy, Together with NO2, NO, and O3 via

559   Cavity Ring-down Spectroscopy. *Environ. Sci. Technol.* **2014**, *48* (16), 9609–9615.

560   https://doi.org/10.1021/es501896w.

561   (43)   Ryerson, T. B.; Huey, L. G.; Knapp, K.; Nueman, J. A.; Parrish, D. D.; Sueper, D. T.;

562   Fehsenfeld, F. C. Design and Initial Characterization of an Inlet for Gas-Phase NOy

563   Measurements from Aircraf. *J. Geophys. Res. Atmos.* **1999**, *104* (D5), 5483–5492.

564   (44)   Brock, C. A.; Schröder, F.; Kärcher, B.; Petzold, A.; Busen, R.; Fiebig, M. Ultrafine

565   Particle Size Distribution Measured in Aircraft Exhaust Plumes. *J. Geophys. Res.* **2000**,

566   *105* (Vi), 26555–26567.

567   (45)   Brock, C. A.; Cozic, J.; Bahreini, R.; Froyd, K. D.; Middlebrook, A. M.; McComiskey,

568   A.; Brioude, J.; Cooper, O. R.; Stohl, A.; Aikin, K. C.; De Gouw, J. A.; Fahey, D. W.;

569   Ferrare, R. A.; Gao, R. S.; Gore, W.; Holloway, J. S.; Hübler, G.; Jefferson, A.; Lack, D.

570   A.; Lance, S.; Moore, R. H.; Murphy, D. M.; Nenes, A.; Novelli, P. C.; Nowak, J. B.;

571   Ogren, J. A.; Peischl, J.; Pierce, R. B.; Pilewskie, P.; Quinn, P. K.; Ryerson, T. B.;

572   Schmidt, K. S.; Schwarz, J. P.; Sodemann, H.; Spackman, J. R.; Stark, H.; Thomson, D.

573   S.; Thornberry, T.; Veres, P.; Watts, L. A.; Warneke, C.; Wollny, A. G. Characteristics,

574   Sources, and Transport of Aerosols Measured in Spring 2008 during the Aerosol,

575   Radiation, and Cloud Processes Affecting Arctic Climate (ARCPAC) Project. *Atmos.*

576   *Chem. Phys.* **2011**, *11* (6), 2423–2453. https://doi.org/10.5194/acp-11-2423-2011.

577   (46)   De Gouw, J.; Warneke, C. Measurements of Volatile Organic Compounds in the Earth's

578   Atmosphere Using Proton-Transfer-Reaction Mass Spectrometry. *Mass Spectrometry*

579   *Reviews*. Wiley-Blackwell March 1, 2007, pp 223–257.

580   https://doi.org/10.1002/mas.20119.

581   (47)   Bond, T. C.; Doherty, S. J.; Fahey, D. W.; Forster, P. M.; Berntsen, T.; Deangelo, B. J.;

582   Flanner, M. G.; Ghan, S.; Kärcher, B.; Koch, D.; Kinne, S.; Kondo, Y.; Quinn, P. K.;

583   Sarofim, M. C.; Schultz, M. G.; Schulz, M.; Venkataraman, C.; Zhang, H.; Zhang, S.;

584   Bellouin, N.; Guttikunda, S. K.; Hopke, P. K.; Jacobson, M. Z.; Kaiser, J. W.; Klimont,

585   Z.; Lohmann, U.; Schwarz, J. P.; Shindell, D.; Storelvmo, T.; Warren, S. G.; Zender, C. S.

586   Bounding the Role of Black Carbon in the Climate System: A Scientific Assessment. *J.*

587   *Geophys. Res. Atmos.* **2013**, *118* (11), 5380–5552. https://doi.org/10.1002/jgrd.50171.

588   (48)   Min, K.-E.; Washenfelder, R. a.; Dubé, W. P.; Langford, a. O.; Edwards, P. M.; Zarzana,

589   K. J.; Stutz, J.; Lu, K.; Rohrer, F.; Zhang, Y.; Brown, S. S. A Broadband Cavity Enhanced

590   Absorption Spectrometer for Aircraft Measurements of Glyoxal, Methylglyoxal, Nitrous

591   Acid, Nitrogen Dioxide, and Water Vapor. *Atmos. Meas. Tech. Discuss.* **2016**, *9* (10),

592   423–440. https://doi.org/10.5194/amtd-8-11209-2015.

593   (49)   Zheng, W.; Flocke, F. M.; Tyndall, G. S.; Swanson, A.; Orlando, J. J.; Roberts, J. M.;

594   Huey, L. G.; Tanner, D. J. Characterization of a Thermal Decomposition Chemical

595   Ionization Mass Spectrometer for the Measurement of Peroxy Acyl Nitrates (PANs) in the

596   Atmosphere. *Atmos. Chem. Phys.* **2011**, *11* (13), 6529–6547. https://doi.org/10.5194/acp-

597   11-6529-2011.

598   (50)   Schwarz, J. P.; Gao, R. S.; Fahey, D. W.; Thomson, D. S.; Watts, L. A.; Wilson, J. C.;

599   Reeves, J. M.; Darbeheshti, M.; Baumgardner, D. G.; Kok, G. L.; Chung, S. H.; Schulz,

600   M.; Hendricks, J.; Lauer, A.; Kärcher, B.; Slowik, J. G.; Rosenlof, K. H.; Thompson, T.

601   L.; Langford, A. O.; Loewenstein, M.; Aikin, K. C. Single-Particle Measurements of

602   Midlatitude Black Carbon and Light-Scattering Aerosols from the Boundary Layer to the

603   Lower Stratosphere. *J. Geophys. Res. Atmos.* **2006**, *111* (16), 1–15.

604   https://doi.org/10.1029/2006JD007076.

605   (51)   Holloway, J. S.; Jakoubek, R. O.; Parrish, D. D.; Gerbig, C.; Volz-Thomas, A.;

606   Schmitgen, S.; Fried, A.; Wert, B.; Henry, B.; Drummond, J. R. Airborne Intercomparison

607   of Vacuum Ultraviolet Fluorescence and Tunable Diode Laser Absorption Measurements

608   of Tropospheric Carbon Monoxide. *J. Geophys. Res. Atmos.* **2000**, *105* (D19), 24251–

609   24261. https://doi.org/10.1029/2000JD900237.

610   (52) Stockwell, C. E.; Veres, P. R.; Williams, J.; Yokelson, R. J. Characterization of Biomass

611   Burning Emissions from Cooking Fires, Peat, Crop Residue, and Other Fuels with High-

612   Resolution Proton-Transfer-Reaction Time-of-Flight Mass Spectrometry. *Atmos. Chem.*

613   *Phys.* **2015**, *15* (2), 845–865. https://doi.org/10.5194/acp-15-845-2015.

614   (53) Kerdouci, J.; Picquet-Varrault, B.; Doussin, J. F. Prediction of Rate Constants for Gas-

615   Phase Reactions of Nitrate Radical with Organic Compounds: A New Structure-Activity

616   Relationship. *ChemPhysChem* **2010**, *11* (18), 3909–3920.

617   https://doi.org/10.1002/cphc.201000673.

618   (54) Edwards, P. M.; Aikin, K. C.; Dube, W. P.; Fry, J. L.; Gilman, J. B.; De Gouw, J. A.;

619   Graus, M. G.; Hanisco, T. F.; Holloway, J.; Hübler, G.; Kaiser, J.; Keutsch, F. N.; Lerner,

620   B. M.; Neuman, J. A.; Parrish, D. D.; Peischl, J.; Pollack, I. B.; Ravishankara, A. R.;

621   Roberts, J. M.; Ryerson, T. B.; Trainer, M.; Veres, P. R.; Wolfe, G. M.; Warneke, C.

622   Transition from High- to Low-NO x Control of Night-Time Oxidation in the Southeastern

623   US. *Nat. Geosci.* **2017**, *10* (7), 490–495. https://doi.org/10.1038/ngeo2976.

624   (55) Wolfe, G. M.; Marvin, M. R.; Roberts, S. J.; Travis, K. R.; Liao, J. The Framework for 0-

625   D Atmospheric Modeling (F0AM) v3.1. *Geosci. Model Dev.* **2016**, *9* (9), 3309–3319.

626   https://doi.org/10.5194/gmd-9-3309-2016.

627   (56) Jenkin, M. E.; Saunders, S. M.; Pilling, M. J. The Tropospheric Degradation of Volatile

628   Organic Compounds: A Protocol for Mechanism Development. *Atmos. Environ.* **1997**, *31*

629   (1), 81–104. https://doi.org/10.1016/S1352-2310(96)00105-7.

630   (57) Jenkin, M. E.; Saunders, S. M.; Wagner, V.; Pilling, M. J. Protocol for the Development

631   of the Master Chemical Mechanism, MCM v3 (Part B): Tropospheric Degradation of

632   Aromatic Volatile Organic Compounds. *Atmos. Chem. Phys.* **2003**, *3* (1), 181–193.

633   https://doi.org/10.5194/acp-3-181-2003.

634 (58) Bloss, C.; Wagner, V.; Jenkin, M. E.; Volkamer, R.; Bloss, W. J.; Lee, J. D.; Heard, D. E.;

635   Wirtz, K.; Martin-Reviejo, M.; Rea, G.; Wenger, J. C.; Pilling, M. J. Development of a

636   Detailed Chemical Mechanism (MCMv3.1) for the Atmospheric Oxidation of Aromatic

637   Hydrocarbons. *Atmos. Chem. Phys.* **2005**, *5* (3), 641–664. https://doi.org/10.5194/acp-5-

638   641-2005.

639 (59) Jenkin, M. E.; Wyche, K. P.; Evans, C. J.; Carr, T.; Monks, P. S.; Alfarra, M. R.; Barley,

640   M. H.; McFiggans, G. B.; Young, J. C.; Rickard, A. R. Development and Chamber

641   Evaluation of the MCM v3.2 Degradation Scheme for β-Caryophyllene. *Atmos. Chem.*

642   *Phys.* **2012**, *12* (11), 5275–5308. https://doi.org/10.5194/acp-12-5275-2012.

643 (60) Jenkin, M. E.; Young, J. C.; Rickard, A. R. The MCM v3.3.1 Degradation Scheme for

644   Isoprene. *Atmos. Chem. Phys.* **2015**, *15* (20), 11433–11459. https://doi.org/10.5194/acp-

645   15-11433-2015.

646 (61) Yang, B.; Zhang, H.; Wang, Y.; Zhang, P.; Shu, J.; Sun, W.; Ma, P. Experimental and

647   Theoretical Studies on Gas-Phase Reactions of NO3 Radicals with Three

648   Methoxyphenols: Guaiacol, Creosol, and Syringol. *Atmos. Environ.* **2016**, *125* (3), 243–

649   251. https://doi.org/10.1016/j.atmosenv.2015.11.028.

650 (62) Tapia, A.; Villanueva, F.; Salgado, M. S.; Cabañas, B.; Martínez, E.; Martín, P.

651   Atmospheric Degradation of 3-Methylfuran: Kinetic and Products Study. *Atmos. Chem.*

652   *Phys.* **2011**, *11* (7), 3227–3241. https://doi.org/10.5194/acp-11-3227-2011.

653 (63) Lauraguais, A.; El Zein, A.; Coeur, C.; Obeid, E.; Cassez, A.; Rayez, M.-T.; Rayez, J.-C.

654   Kinetic Study of the Gas-Phase Reactions of Nitrate Radicals with Methoxyphenol

655   Compounds: Experimental and Theoretical Approaches. *J. Phys. Chem. A* **2016**, *120* (17),

656   2691–2699. https://doi.org/10.1021/acs.jpca.6b02729.

657 (64) CropScape - NASS CDL Program https://nassgeodata.gmu.edu/CropScape/ (accessed Aug

658   6, 2018).

659 (65) Brown, S. Absorption Spectroscopy in High Finesse Cavities for Atmospheric Studies.

660   *Chem. Rev.* **2003**, *103*, 5219.

661 (66) Brown, S. S.; Stark, H.; Ravishankara, A. R. Applicability of the Steady State

662   Approximation to the Interpretation of Atmospheric Observations of NO 3 and N 2 O 5. *J.*

663   *Geophys. Res.* **2003**, *108* (D17), 4539. https://doi.org/10.1029/2003JD003407.

664 (67) Olariu, R. I.; Bejan, I.; Barnes, I.; Klotz, B.; Becker, K. H.; Wirtz, K. Rate Coefficients for

665   the Gas-Phase Reaction of NO3 Radicals with Selected Dihydroxybenzenes. *Int. J. Chem.*

666   *Kinet.* **2004**, *36* (11), 577–583. https://doi.org/10.1002/kin.20029.

667 (68) Finewax, Z.; De Gouw, J. A.; Ziemann, P. J. Identification and Quantification of 4-

668   Nitrocatechol Formed from OH and NO3Radical-Initiated Reactions of Catechol in Air in

669   the Presence of NOx: Implications for Secondary Organic Aerosol Formation from

670   Biomass Burning. *Environ. Sci. Technol.* **2018**, *52* (4), 1981–1989.

671   https://doi.org/10.1021/acs.est.7b05864.

672 (69) Desyaterik, Y.; Sun, Y.; Shen, X.; Lee, T.; Wang, X.; Wang, T.; Collett, J. L. Speciation

673   of "Brown" Carbon in Cloud Water Impacted by Agricultural Biomass Burning in Eastern

674   China. *J. Geophys. Res. Atmos.* **2013**, *118* (13), 7389–7399.

675   https://doi.org/10.1002/jgrd.50561.

676 (70) Claeys, M.; Vermeylen, R.; Yasmeen, F.; Gómez-González, Y.; Chi, X.; Maenhaut, W.;

677   Mészáros, T.; Salma, I. Chemical Characterisation of Humic-like Substances from Urban,

678   Rural and Tropical Biomass Burning Environments Using Liquid Chromatography with

679   UV/Vis Photodiode Array Detection and Electrospray Ionisation Mass Spectrometry.

680   *Environ. Chem.* **2012**, *9* (3), 273–284. https://doi.org/10.1071/EN11163.

681 (71) Lin, P.; Bluvshtein, N.; Rudich, Y.; Nizkorodov, S. A.; Laskin, J.; Laskin, A. Molecular

682   Chemistry of Atmospheric Brown Carbon Inferred from a Nationwide Biomass Burning

683   Event. *Environ. Sci. Technol.* **2017**, *51* (20), 11561–11570.

684   https://doi.org/10.1021/acs.est.7b02276.

685 (72) Iinuma, Y.; Boge, O.; Grade, R.; Herrmann, H. Methyl-Nitrocatechols : Atmospheric

686   Tracer Compounds for Biomass Burning Secondary Organic Aerosols. *Environ. Sci.*

687   *Technol.* **2010**, *44*, 8453–8459.

688 (73) Gaston, C. J.; Lopez-Hilfiker, F. D.; Whybrew, L. E.; Hadley, O.; McNair, F.; Gao, H.;

689   Jaffe, D. A.; Thornton, J. A. Online Molecular Characterization of Fine Particulate Matter

690   in Port Angeles, WA: Evidence for a Major Impact from Residential Wood Smoke.

691   *Atmos. Environ.* **2016**, *138*, 99–107. https://doi.org/10.1016/j.atmosenv.2016.05.013.

692 (74) Mohr, C.; Lopez-Hilfiker, F. D.; Zotter, P.; Prévoît, A. S. H.; Xu, L.; Ng, N. L.; Herndon,

693   S. C.; Williams, L. R.; Franklin, J. P.; Zahniser, M. S.; Worsnop, D. R.; Knighton, W. B.;

694   Aiken, A. C.; Gorkowski, K. J.; Dubey, M. K.; Allan, J. D.; Thornton, J. A. Contribution

695   of Nitrated Phenols to Wood Burning Brown Carbon Light Absorption in Detling, United

696   Kingdom during Winter Time. *Environ. Sci. Technol.* **2013**, *47* (12), 6316–6324.

697   https://doi.org/10.1021/es400683v.

698 (75) Xie, M.; Chen, X.; Hays, M. D.; Lewandowski, M.; Offenberg, J.; Kleindienst, T. E.;

699   Holder, A. L. Light Absorption of Secondary Organic Aerosol: Composition and

700   Contribution of Nitroaromatic Compounds. *Environ. Sci. Technol.* **2017**, *51* (20), 11607–

701   11616. https://doi.org/10.1021/acs.est.7b03263.

702 (76) Hinrichs, R. Z.; Buczek, P.; Trivedi, J. J. Solar Absorption by Aerosol-Bound

703   Nitrophenols Compared to Aqueous and Gaseous Nitrophenols. *Environ. Sci. Technol.*

704   **2016**, *50* (11), 5661–5667. https://doi.org/10.1021/acs.est.6b00302.

705 (77) Odum Jay, R.; Hoffmann, T.; Bowman, F.; Collins, D.; Flagan Richard, C.; Seinfeld John,

706   H. Gas Particle Partitioning and Secondary Organic Aerosol Yields. *Environ. Sci.*

707   *Technol.* **1996**, *30* (8), 2580–2585. https://doi.org/10.1021/es950943+.

708